

Doping-induced incommensurate antiferromagnetism in a Mott-Hubbard insulator

E. Arrigoni and G. C. Strinati
Scuola Normale Superiore, I-56100 Pisa, Italy
 (Received 24 April 1991)

Properties of incommensurate spiral spin phases are calculated at the mean-field level for a single-band Hubbard Hamiltonian with variable hole density, by adapting both the Hartree-Fock decoupling and the Kotliar-Ruckenstein slave-boson approach to a regular twist of the spin quantization axes from site to site in a two-dimensional square lattice. The relative stability of the (1,1) and (1,0) spiral phases, the coexistence of the antiferromagnetic and the spiral phases over a finite range of hole density, and the stiffness of the spirals against fluctuations of their direction and pitch are discussed within the model Hamiltonian over a wide range of hole density and interaction strength.

I. INTRODUCTION

The occurrence of incommensurate antiferromagnetism in strongly correlated fermion systems has been an argument of considerable recent theoretical interest,¹⁻⁸ in the effort to relate the interpretation of the physical properties of high-temperature superconducting materials to a theoretical understanding of the normal-state properties of strongly correlated fermion systems. This effort has been prompted by the experimental report of incommensurate antiferromagnetism in CuO₂-based high-temperature superconducting samples of La_{2-x}Sr_xCuO_{4-y}.⁹ Since it is also established that the La₂CuO₄ parent compound is a commensurate (Neél) antiferromagnet, the incommensurate distortion of the spin order has been ascribed to the system trying to adapt to the addition of holes in the CuO₂ planes upon doping. Experiments have further indicated that incommensurate order shows up when doping exceeds a threshold which turns out to coincide with the minimal doping for superconductivity to occur.⁹ Although the coincidence of the two thresholds may simply support the idea that both phenomena are independently related to the hole mobility, people have unavoidably been led to speculate that the spin state associated with incommensurability is a prerequisite for superconductivity to exist. A connection (if any) between the two phenomena, however, has not yet been established.

Pending this connection, it is worthwhile to study the properties of the incommensurate spin state *per se* in some detail. In this paper we shall, in particular, consider the competition between the antiferromagnetic and the spiral incommensurate phases upon doping. Several questions can be addressed in this context. Specifically, we will inquire about (i) the existence of various spiral phases which may become energetically favored in different doping ranges; (ii) the occurrence of a phase separation in hole-rich and no-hole phases which coexist in a well-defined doping range where the homogeneous phases are intrinsically unstable; and (iii) the stability of the spiral phases against fluctuations in the direction and in the pitch of the spirals. We remark that question (i) be-

comes relevant whenever question (ii) can be affirmed, because in this case the incommensurate phase present at small doping could have only a finite pitch corresponding to a phase stable at larger doping. We note, however, that our discussion about the intrinsic instability of the homogeneous phases against phase separation will be restricted by neglecting additional physical effects (such as the long-range repulsion among the holes) which could effectively prevent it unless properly balanced (for instance, by screening effects).¹⁰ Question (iii) hinges instead on the spiral phases being envisaged as the underlying structures for the construction of moment-free quantum spin nematics in the presence of large quantum fluctuations.¹¹

We base our calculations on a two-dimensional single-band Hubbard model because we expect this model to capture the essential physics present in the magnetic properties of the high-temperature superconductors. We perform two types of mean-field calculations based on different decouplings of the Hubbard Hamiltonian for itinerant holes, with the intent to cover a wide interaction range from weak to strong coupling. We begin by considering a local magnetic Hartree-Fock decoupling along spin quantization axes that twist regularly from site to site of the two-dimensional square lattice, thereby yielding a spiral spin pattern with constant direction and uniform pitch. We are able in this way to reproduce the numerical results obtained recently by Schulz⁷ via an effective action derived through functional integral methods. We extend Schulz's results further by noticing the occurrence of a discontinuous transition from the (1,1) to the (1,0) incommensurate phases at finite doping. For intermediate values of the Mott-Hubbard parameter U/t we also find that the incommensurate phases are unstable against phase separation in a doping range which is relevant to ceramic superconductors. We study next the incommensurate phases via a mean-field slave-boson approach which adapts the Kotliar and Ruckenstein formulation¹² when the spin quantization axes are regularly twisting from site to site. Consistently with one's expectation that the slave-boson approach is better suited than an ordinary Hartree-Fock decoupling in the

intermediate- and strong-coupling regimes, we now find the incommensurate phases to be stable over a considerably wider doping range.

We have mentioned already that incommensurate spiral phases have been discussed by several authors.^{1-2,4,6-8} These calculations, however, have been based on the t - J model (or its variations) which can be derived from the Hubbard model when U/t is large compared to unity. Our findings of a transition between the incommensurate spiral phases (1,1) and (1,0) at finite doping and of an intrinsic range of stability of these phases, both occurring rather at intermediate values of U/t , were thus precluded to those calculations based on the t - J model.

The plan of the paper is the following. In Sec. II we formulate the Hartree-Fock decoupling for spin spirals by allowing the spin quantization axis to be site dependent via a suitable transformation of the spin- $\frac{1}{2}$ operators. The straightforward calculation which results suffices to establish general trends for the relative stability of the incommensurate phases. In Sec. III the same questions are faced with the slave-boson approach. Section IV gives our conclusions. In Appendix A we describe the Maxwell construction which identifies the doping range where the antiferromagnetic and the spiral phases can coexist in equilibrium, owing to an anomalous decrease of the chemical potential with increasing particle number. In Appendix B we finally show that the averaging over all possible realizations of the site-dependent spin quantization axes suffices to render the Kotliar-Ruckenstein slave-boson approach manifestly spin-rotationally invariant.

II. HARTREE-FOCK DECOUPLING WITH TWISTING SPIN QUANTIZATION AXES

We begin by considering a single-band Hubbard Hamiltonian for a two-dimensional square lattice (in hole notation)

$$H = (\varepsilon_0 - \mu) \sum_{i,\sigma} c_{i\sigma}^\dagger c_{i\sigma} + t \sum_{\langle ij \rangle} \left[\sum_{\sigma} c_{i\sigma}^\dagger c_{j\sigma} + \text{H.c.} \right] + U \sum_i c_{i\uparrow}^\dagger c_{i\uparrow} c_{i\downarrow}^\dagger c_{i\downarrow}, \quad (2.1)$$

where ε_0 is the site energy, μ the chemical potential, the double lattice sum is limited to pairs of neighboring sites, and the spin projection σ refers to a common (say, \hat{z}) quantization axis. Although a more realistic multiband Hubbard model could be considered with no difficulty, we regard the simplified Hamiltonian (2.1) sufficient to discuss the variety of magnetic phases we are interested in.

Spin-symmetry breaking on the Hamiltonian (2.1) can be achieved as follows. For each pair $(c_{i\uparrow}, c_{i\downarrow})$ of destruction operators at a given lattice site i , we introduce the unitary transformation

$$d_{i\xi} = \sum_{\sigma} [\mathcal{R}^\dagger(\Omega_i)]_{\xi\sigma} c_{i\sigma}, \quad (2.2)$$

where

$$\mathcal{R}(\Omega_i) = e^{-i(\varphi_i/2)\sigma_z} e^{-i(\theta_i/2)\sigma_y} \quad (2.3)$$

is the rotation operator which (apart from a phase) transforms the eigenvectors of the Pauli spin matrix σ_z into the eigenvectors of the matrix $\sigma(\Omega_i) = \sin\theta_i(\cos\varphi_i\sigma_x + \sin\varphi_i\sigma_y) + \cos\theta_i\sigma_z$ along the local quantization axis specified by the spherical angles $\Omega_i \equiv (\theta_i, \varphi_i)$. Suppose that the set of angles $\{\Omega_i\}$ is specified for all lattice sites. The Hamiltonian (2.1) can then be transformed into an equivalent form that takes explicitly into account the set of variable quantization axes:

$$H(\{\Omega_i\}) = (\varepsilon_0 - \mu) \sum_{i,\xi} d_{i\xi}^\dagger d_{i\xi} + t \sum_{\langle ij \rangle} \left[\sum_{\xi,\xi'} d_{i\xi}^\dagger [\mathcal{R}^\dagger(\Omega_i)\mathcal{R}(\Omega_j)]_{\xi\xi'} d_{j\xi'} + \text{H.c.} \right] + U \sum_i d_{i+}^\dagger d_{i+} + d_{i-}^\dagger d_{i-}. \quad (2.4)$$

The invariance of the interaction term in (2.1) under the transformation (2.2) is readily verified by writing

$$c_{i\uparrow}^\dagger c_{i\uparrow} c_{i\downarrow}^\dagger c_{i\downarrow} = \frac{1}{2} [(c_{i\uparrow}^\dagger c_{i\uparrow} + c_{i\downarrow}^\dagger c_{i\downarrow})^2 - (c_{i\uparrow}^\dagger c_{i\uparrow} - c_{i\downarrow}^\dagger c_{i\downarrow})] \quad (2.5)$$

and noticing that

$$c_{i\uparrow}^\dagger c_{i\uparrow} + c_{i\downarrow}^\dagger c_{i\downarrow} = d_{i+}^\dagger d_{i+} + d_{i-}^\dagger d_{i-} \quad (2.6)$$

since the transformation (2.3) is unitary.

The mean-field Hartree-Fock decoupling of the Hamiltonian (2.4) is obtained at this point by the usual one-body reduction of the interaction term:

$$U \sum_i d_{i+}^\dagger d_{i+} + d_{i-}^\dagger d_{i-} \rightarrow U \sum_{i,\xi} m_{i\xi} d_{i\xi}^\dagger d_{i\xi} - U \sum_i m_{i+} + m_{i-}, \quad (2.7)$$

where the (zero-temperature) average

$$m_{i\xi} = \langle d_{i\xi}^\dagger d_{i\xi} \rangle \quad (2.8)$$

has to be self-consistently determined.

Despite the local variable quantization axes, the Hamiltonian (2.4) with the replacement (2.7) can be diagonalized by Bloch transforming the set of operators $\{d_{i\xi}; i=1,2,\dots,N\}$ (N being the number of lattice sites), provided

(i) the set of local quantization axes displays a regular order, in the sense that each product $\mathcal{R}^\dagger(\Omega_i)\mathcal{R}(\Omega_j)$ depends actually on $\mathbf{R}_i - \mathbf{R}_j$ and not on \mathbf{R}_i and \mathbf{R}_j separately, where \mathbf{R}_i is the lattice vector associated with site i ,¹³

(ii) the average (2.8) along the local quantization axis is site independent.¹⁴

Since the two operators on the right-hand side of Eq. (2.3) do not commute, condition (i) is fulfilled by setting $\varphi_i = 0$ and choosing

$$\theta_i = \mathbf{Q} \cdot \mathbf{R}_i, \quad (2.9)$$

where \mathbf{Q} is a wave vector belonging to the Brillouin zone. With this choice we obtain

$$\mathcal{R}^\dagger(\Omega_i)\mathcal{R}(\Omega_j) = e^{i[\mathbf{Q}\cdot(\mathbf{R}_i - \mathbf{R}_j)\sigma_y]/2}. \quad (2.10)$$

Condition (ii) implies instead

$$m_{i\xi} = m_1 + \xi m_2, \quad (2.11)$$

where different occupations for the two local spin components have been allowed.

With the Bloch transformation

$$d_{\mathbf{k}\xi} = \frac{1}{\sqrt{N}} \sum_i e^{-i\mathbf{k}\cdot\mathbf{R}_i} d_{i\xi}, \quad (2.12)$$

the Hartree-Fock Hamiltonian then reduces now to the simple form

$$\begin{aligned} H(\mathbf{Q}) = & \sum_{\mathbf{k}} \sum_{\xi, \xi'} d_{\mathbf{k}\xi}^\dagger [(tT_e(\mathbf{k}, \mathbf{Q}) + \varepsilon_0 - \mu + Um_1)I \\ & + tT_o(\mathbf{k}, \mathbf{Q})\sigma_y - Um_2\sigma_z]_{\xi\xi'} d_{\mathbf{k}\xi'} \\ & - UN(m_1^2 - m_2^2), \end{aligned} \quad (2.13)$$

where I stands for the 2×2 unit matrix and we have defined

$$T_e(\mathbf{k}, \mathbf{Q}) = 2 \left[\cos(k_x a) \cos \left[\frac{Q_x a}{2} \right] + \cos(k_y a) \cos \left[\frac{Q_y a}{2} \right] \right], \quad (2.14a)$$

$$T_o(\mathbf{k}, \mathbf{Q}) = 2 \left[\sin(k_x a) \sin \left[\frac{Q_x a}{2} \right] + \sin(k_y a) \sin \left[\frac{Q_y a}{2} \right] \right] \quad (2.14b)$$

(a being the lattice constant). Notice that the expressions (2.14) are invariant when the operations belonging to the point group C_{4v} of the two-dimensional square lattice are simultaneously applied to \mathbf{k} and \mathbf{Q} . This implies that, while the total energy $E(\mathbf{Q})$ has the symmetry of the square lattice, the single-particle eigenvalues $\varepsilon_n(\mathbf{k}, \mathbf{Q})$ do not preserve the full \mathbf{k} symmetry for a generic \mathbf{Q} .

The chemical potential can be eliminated at this point in favor of the doping parameter δ by the (zero temperature) condition

$$\frac{1}{N} \sum_{\mathbf{k}} \sum_n \theta(\mu - \varepsilon_n(\mathbf{k}, \mathbf{Q})) = 1 + \delta, \quad (2.15)$$

where $\theta(x)$ is the unit-step function, while the optimum value of the wave vector \mathbf{Q} is determined, as in the corresponding classical spin-wave theory,¹⁵ by minimizing the total energy. The spin structures of interest are thus realized as follows:

- (i) paramagnetic, $m_2 = 0$ and \mathbf{Q} undetermined;
- (ii) antiferromagnetic, $m_2 \neq 0$ and $\mathbf{Q}_{AF} = (\pi/a)(1, 1)$;
- (iii) ferromagnetic, $m_2 \neq 0$ and $\mathbf{Q}_F = (0, 0)$;
- (iv) spiral, $m_2 \neq 0$ and $\mathbf{Q} = (Q_x, Q_y)$ ranging in the irreducible wedge of the Brillouin zone.

It turns out that that one can consider only the *diagonal* [$\mathbf{Q} = \mathbf{Q}_{AF} + \Delta\mathbf{Q}(1, 1)$] and *transverse* [$\mathbf{Q} = \mathbf{Q}_{AF} + \Delta\mathbf{Q}(1, 0)$] directions, which correspond to the diagonal and the boundary of the irreducible wedge, respectively. Numerical calculations show, in fact, that the energy

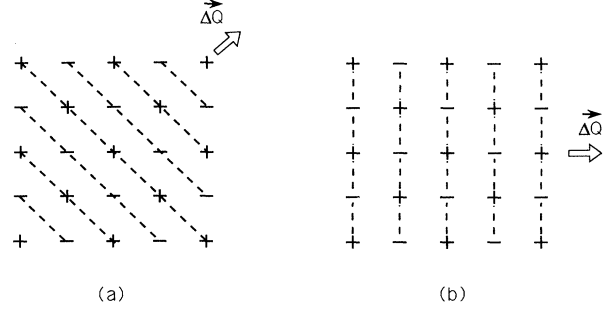


FIG. 1. + and - marks identify opposite spin orientations at zero doping. Dashed lines join spins which share the same twisting angle upon doping since $\Delta\mathbf{Q}\cdot\mathbf{R}_i = \text{const}$ along these lines. (a) For the diagonal spiral phase and (b) for the transverse spiral phase.

minimum occurs along either one of these special directions over the wide ranges of U/t and δ we have explored. Starting from the antiferromagnetic solution at half-filling ($\delta = 0$), for increasing doping we notice that the diagonal spiral phase preserves the ferromagnetic alignment between half of the second nearest neighbors while the transverse spiral phase preserves the antiferromagnetic alignment between half of the first nearest neighbors (see Fig. 1).

In Fig. 2 the spiral pitch parameter $a\Delta\mathbf{Q}/\pi$ corresponding to the diagonal (1,1) phase is plotted versus doping δ and t/U in the strong interaction regime ($U/t \geq 5$). Notice, in particular, the rapid evolution from the antiferromagnetic ($\Delta\mathbf{Q} = 0$) to the ferromagnetic ($\Delta\mathbf{Q} = \pi/a$) phase which occurs for small values of δ and t/U . Comparison between our Fig. 2 and an analogous figure by Schulz⁷ shows that the present Hartree-Fock calculation is able to reproduce (to within a

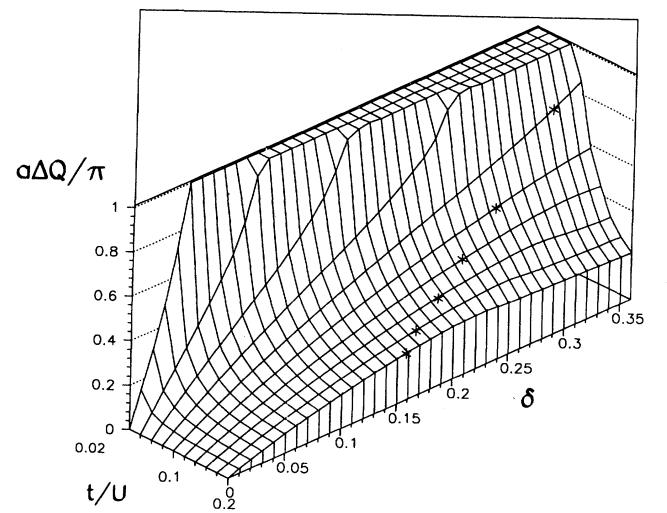


FIG. 2. Spiral pitch parameter $a\Delta\mathbf{Q}/\pi$ for the (1,1) phase vs doping δ and inverse strength of correlation t/U in the strong interaction regime of the Hartree-Fock approximation. Stars identify the critical doping δ_c at fixed t/U for which a first-order transition to the (1,0) phase occurs.

10–20 % accuracy) Schultz's results which have been obtained via an effective action appropriate to the strongly correlated case. Figure 2 locates, in addition, the critical doping δ_c (at fixed t/U) beyond which the diagonal (1,1) phase is no longer energetically favored with respect to the transverse (1,0) phase. For small values of t/U ($\lesssim 0.09$), however, the continuous transition from the (1,1) spiral directly to the ferromagnetic phase is preferred. For larger values of t/U ($\gtrsim 0.11$) and larger doping than shown in Fig. 2, the paramagnetic phase has instead the lowest energy.

In the weak and intermediate interaction regimes ($U/t \lesssim 5$) the transition from the (1,1) to the (1,0) spiral phase occurs at smaller doping. A plot of the corresponding critical doping in this region is shown in Fig. 3.

The vanishing of the spiral pitch parameter at small doping over the whole range of t/U shown in Fig. 2 should mean that the antiferromagnetic phase is energetically favored at half-filling, with the spiral phases developing with continuity from the antiferromagnetic phase for increasing doping. Physically, the spiral phases are preferred for increasing doping because the kinetic energy of the holes can lower the total energy when neighboring spins are not completely antiparallel.¹⁶ Irrespective of the continuity of the spiral pitch parameter at small doping, however, the present calculation implies that the spiral phases do not actually evolve continuously from the antiferromagnetic phase at half-filling; rather, the two phases coexist in equilibrium from half-filling to a critical doping (say, δ^*) with the system undergoing a first-order phase transition. To show this we report in Fig. 4 the behavior of the chemical potential $\mu(\delta)$ versus δ for the two spiral phases (1,1) and (1,0) and for two representative values of U/t : in all cases, $\mu(\delta)$ suffers initially an unphysical decrease from the bottom of the empty antiferromagnetic band at $\delta=0^+$ down to a minimum at $\delta=\delta_m$. As is usually the case, we ascribe the occurrence of a doping range where $d\mu(\delta)/d\delta$ is negative to the implicit assumption of our calculation that the spiral phases are homogeneous, with no allowance made for the possible coexistence of two phases. To improve on this situation we can perform a Maxwell construction in the manner indicated in Appendix A, thereby inquiring whether two

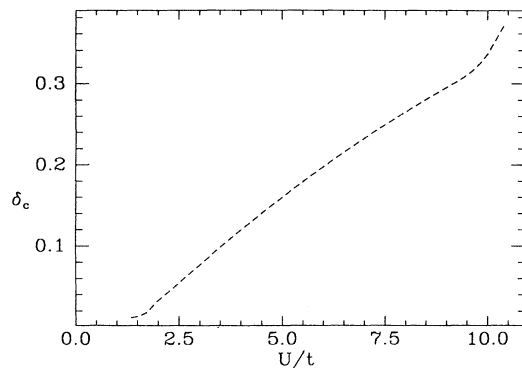


FIG. 3. Critical doping δ_c for the transition from the (1,1) to the (1,0) spiral phase vs U/t in the weak and intermediate interaction regimes of the Hartree-Fock approximation.

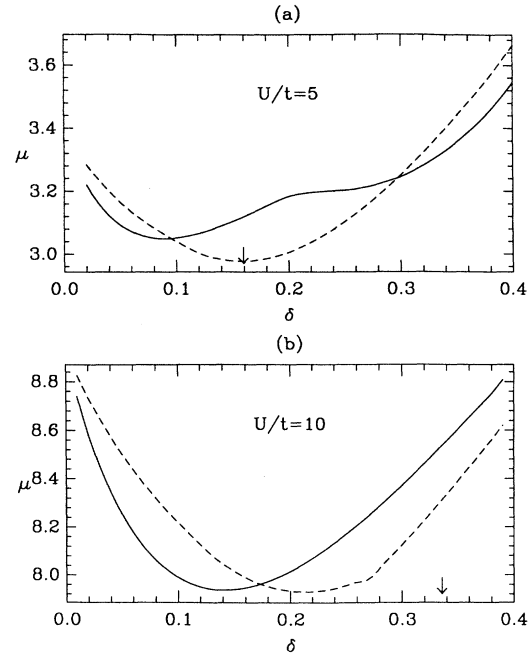


FIG. 4. Chemical potential (in units of t) vs doping when (a) $U/t=5$ and (b) $U/t=10$ in the Hartree-Fock approximation. Solid and broken lines refer to the (1,1) and (1,0) spiral phases, respectively, and the arrows locate the critical doping δ_c where the transition (1,1)→(1,0) occurs (see text). [We notice that the abrupt change of slope occurring in (b) for the (1,0) phase corresponds to the transition to a state which is ferromagnetic along ΔQ and antiferromagnetic orthogonally to ΔQ .] The zero of the chemical potential has been set at the top of the lower filled band at zero doping.

different states (namely, the antiferromagnetic and the spiral state with the well-defined pitch parameter $a \Delta Q^*/\pi$) can coexist in equilibrium when $0 \leq \delta \leq \delta^*$. For the cases of Fig. 4, in particular, we obtain $\delta^* \approx 0.24$ and $\delta^* \approx 0.23$, in the order, with δ^* belonging to the stability domain of the (1,0) and of the (1,1) phases in the two cases. For $\delta > \delta^*$ the homogeneous spiral phase (with the value of ΔQ appropriate to the doping δ) becomes thermodynamically stable.

We emphasize again that the whole discussion about phase separation is meaningful *provided* the holes are not prevented from separating into a no-hole and into a hole-rich phase by additional physical effects not included in the present model.¹⁰

It is convenient to postpone the discussion of more detailed features of the spiral phases to the next section within an alternative mean-field calculation.

III. SLAVE-BOSON APPROACH WITH TWISTING SPIN QUANTIZATION AXES

The Hartree-Fock calculation discussed in Sec. II suffices to signal the existence of two competing spiral phases and of a threshold for their stability as homogeneous phases. We expect, however, that the known tenden-

cy of the Hartree-Fock approximation to overestimate the occurrence of the ferromagnetic (Stoner) phase¹⁷ results in a sizable compression for the stability domain of the spiral phases in the $(\delta, U/t)$ plane. To get a more quantitative behavior for these phases, we then adopt a different mean-field approach based on the slave-boson method by Kotliar and Ruckenstein,¹² which is believed to be well suited to describe highly correlated electron systems. It has further been shown that the antiferromagnetic mean-field approximation to the Kotliar-Ruckenstein method for a two-dimensional single-band Hubbard model leads to quantitative agreement with Monte Carlo results over a wide range of doping and interaction strength.¹⁸

We begin by reconsidering the Hamiltonian (2.4) for a set of variable quantization axes directed locally along Ω_i . Following the original formulation by Kotliar and Ruckenstein,¹² we then assign to each site i a set of four slave bosons which specify empty (e_i), singly occupied ($s_{i\xi}$), and doubly occupied (D_i) states. As in Sec. II, the

label ξ refers to the spin orientation along the local quantization axis. To avoid unphysical multiple occupancy by slave bosons at a given site, two constraints must be supplemented which project onto the physical subspace at each site:

$$\begin{aligned} \text{(I)} \quad & e_i^\dagger e_i + \sum_{\xi} s_{i\xi}^\dagger s_{i\xi} + D_i^\dagger D_i = 1, \\ \text{(II)} \quad & d_{i\xi}^\dagger d_{i\xi} = s_{i\xi}^\dagger s_{i\xi} + D_i^\dagger D_i. \end{aligned} \quad (3.1)$$

In practice, these constraints are enforced by introducing Lagrange multiplier fields, λ_i^I and $\lambda_{i\xi}^{II}$ in the order, at each site, thereby adding two new terms to the transformed Hamiltonian. The latter is obtained from Eq. (2.4) by mapping the fermionic operator $d_{i\xi}$ into

$$d_{i\xi} \rightarrow z_{i\xi} d_{i\xi}, \quad (3.2)$$

where $z_{i\xi}$ is a bosonic operator to be specified below. One gets

$$\begin{aligned} H(\{\Omega_i\}) = & (\varepsilon_0 - \mu) \sum_{i,\xi} d_{i\xi}^\dagger d_{i\xi} + t \sum_{\langle ij \rangle} \left[\sum_{\xi,\xi'} d_{i\xi}^\dagger z_{i\xi}^\dagger [\mathcal{R}^\dagger(\Omega_i) \mathcal{R}(\Omega_j)]_{\xi\xi'} z_{j\xi'} d_{j\xi'} + \text{H.c.} \right], \\ & + U \sum_i D_i^\dagger D_i - \sum_i \lambda_i^I \left[e_i^\dagger e_i + \sum_{\xi} s_{i\xi}^\dagger s_{i\xi} + D_i^\dagger D_i - 1 \right] - \sum_{i,\xi} \lambda_{i\xi}^{II} (d_{i\xi}^\dagger d_{i\xi} - s_{i\xi}^\dagger s_{i\xi} - D_i^\dagger D_i). \end{aligned} \quad (3.3)$$

Because of the constraints (3.1), the mapping (3.2) is not unique. In particular, any choice of the type

$$z_{i\xi} = e_i^\dagger F(e_i, s_{i\xi}, D_i) s_{i\xi} + s_{i\xi}^\dagger F(e_i, s_{i\xi}, D_i) D_i \quad (3.4)$$

leads to a faithful mapping provided the function $F(e_i, s_{i\xi}, D_i)$ of the slave-boson operators is equivalent to the identity when (3.4) acts within the physical subspace. Kotliar and Ruckenstein¹² have shown that the choice

$$F(e_i, s_{i\xi}, D_i) = \frac{1}{\sqrt{1 - D_i^\dagger D_i - s_{i\xi}^\dagger s_{i\xi}} \sqrt{1 - e_i^\dagger e_i - s_{i\xi}^\dagger s_{i\xi}}} \quad (3.5)$$

reproduces the independent-particle limit ($U=0$) within the mean-field approximation to a single-band Hubbard model. Although it is not evident *a priori* that the choice (3.5) can also apply to a strongly correlated system with broken spin symmetry, we have previously shown¹⁹ at the mean-field level for a multiband Hubbard Hamiltonian that the choice (3.5) reproduces both the energy of the antiferromagnetic (Néel) state in the localized limit (when comparison with perturbation theory is meaningful) and the corresponding clustering of the Néel state into molecular-like orbitals. We therefore adopt the choice (3.5) also in the present context.

A mean-field approximation is obtained from the Hamiltonian (3.3) by replacing all bosonic operators therein

with real numbers to be determined self-consistently. If we further regard these numbers and the Lagrange multipliers as being site independent and limit the product $\mathcal{R}^\dagger(\Omega_i) \mathcal{R}(\Omega_j)$ to the form (2.10), we can exploit the Bloch transformation (2.12) to rewrite the mean-field Hamiltonian in the simple form

$$\begin{aligned} H(\mathbf{Q}) = & \sum_{\mathbf{k}} \sum_{\xi,\xi'} d_{\mathbf{k}\xi}^\dagger [M(\mathbf{k}, \mathbf{Q})]_{\xi\xi'} d_{\mathbf{k}\xi'} \\ & + UN D^2 - N \lambda^I \left[e^2 + \sum_{\xi} s_{\xi}^2 + D^2 - 1 \right] \\ & + N \sum_{\xi} \lambda_{\xi}^{II} (s_{\xi}^2 + D^2), \end{aligned} \quad (3.6)$$

where

$$[M(\mathbf{k}, \mathbf{Q})]_{++} = tz_+^2 T_e(\mathbf{k}, \mathbf{Q}) + \varepsilon_0 - \mu - \lambda_+^{II}, \quad (3.7a)$$

$$\begin{aligned} [M(\mathbf{k}, \mathbf{Q})]_{+-} &= M(\mathbf{k}, \mathbf{Q})_{*+} \\ &= -itz_+ z_- T_o(\mathbf{k}, \mathbf{Q}), \end{aligned} \quad (3.7b)$$

$$[M(\mathbf{k}, \mathbf{Q})]_{--} = tz_-^2 T_e(\mathbf{k}, \mathbf{Q}) + \varepsilon_0 - \mu - \lambda_-^{II}, \quad (3.7c)$$

with the notation (2.14). Let $[V(\mathbf{k}, \mathbf{Q})]_{\xi n}$ be the unitary matrix which diagonalizes $[M(\mathbf{k}, \mathbf{Q})]_{\xi\xi'}$. The mean-field parameters are then self-consistently determined through the equations

$$e^2 + s_+^2 + s_-^2 + D^2 = 1, \quad s_+^2 + s_-^2 + 2D^2 = 1 + \delta,$$

$$s_+^2 - s_-^2 = m_s = \frac{1}{N} \sum_{\mathbf{k}} \sum_n^{\text{BZ}} \theta(\mu - \varepsilon_n(\mathbf{k}, \mathbf{Q})) \{ [V^\dagger(\mathbf{k}, \mathbf{Q})]_{n+} [V(\mathbf{k}, \mathbf{Q})]_{+n} - [V^\dagger(\mathbf{k}, \mathbf{Q})]_{n-} [V(\mathbf{k}, \mathbf{Q})]_{-n} \},$$

$$\frac{1}{N} \sum_{\mathbf{k}} \sum_n^{\text{BZ}} \theta(\mu - \varepsilon_n(\mathbf{k}, \mathbf{Q})) \sum_{\xi, \xi'} [V^\dagger(\mathbf{k}, \mathbf{Q})]_{n\xi} \frac{\partial}{\partial b} [M(\mathbf{k}, \mathbf{Q})]_{\xi\xi'} [V(\mathbf{k}, \mathbf{Q})]_{\xi'n} + \frac{\partial}{\partial b} \left[UD^2 - \lambda^I \left(e^2 + \sum_{\xi} s_{\xi}^2 + D^2 - 1 \right) + \sum_{\xi} \lambda_{\xi}^{\text{II}} (s_{\xi}^2 + D^2) \right] = 0. \quad (3.8)$$

In these expressions, m_s is the local magnetic moment, $\varepsilon_n(\mathbf{k}, \mathbf{Q})$ are band eigenvalues for given \mathbf{Q} , and b stands for any of the four bosons (e, s_+, s_-, D). The chemical potential can again be eliminated in favor of the doping parameter δ via Eq. (2.15). Finally, minimization of the total energy with respect to the wave vector \mathbf{Q} can be achieved by complementing Eqs. (3.8) with the following self-consistency equation:

$$\frac{1}{N} \sum_{\mathbf{k}} \sum_n^{\text{BZ}} \theta(\mu - \varepsilon_n(\mathbf{k}, \mathbf{Q})) \sum_{\xi, \xi'} [V^\dagger(\mathbf{k}, \mathbf{Q})]_{n\xi} \nabla_{\mathbf{Q}} [M(\mathbf{k}, \mathbf{Q})]_{\xi\xi'} [V(\mathbf{k}, \mathbf{Q})]_{\xi'n} = 0. \quad (3.9)$$

Figure 5 gives the spiral pitch parameter $a\Delta Q/\pi$ versus doping for the (1,1) diagonal and (1,0) transverse phases and for two characteristic values of U/t . Hartree-Fock results are also shown for comparison. Notice that the slave-boson approach results in a slower increase of ΔQ at small doping and in a decrease of ΔQ after a maximum at intermediate doping while approaching the paramagnetic phase.

The energy gain per site relative to the antiferromagnetic phase is shown in Fig. 6 versus doping for either one of the two homogeneous spiral phases. The vanishing of the energy gain at large doping corresponds to a decrease of the local magnetic moment m_s for all phases. Notice that the (absolute) value of this energy gain ($\lesssim 10^{-2}t$) is one order of magnitude smaller than the typ-

ical overall gain due to magnetic interactions ($\lesssim 10^{-1}t$) for a two-dimensional Hubbard Hamiltonian. From Fig. 6 one can also locate the critical doping δ_c for the transition from the (1,1) to the (1,0) spiral phases.

A plot of δ_c for smaller values of U/t shown in Fig. 7, where the Hartree-Fock results of Fig. 3 are also reported for comparison. Typically, $\delta_c^{\text{HF}}/\delta_c^{\text{SB}} \approx \frac{2}{3}$ when $2 \lesssim U/t \lesssim 5$.

The anomalous decrease of the chemical potential with doping, which was pointed out in Sec. II within the Hartree-Fock decoupling, occurs also in the slave-boson approach as evidenced in Fig. 8. Comparison with the analogous Hartree-Fock results of Fig. 4 shows that the doping range has been compressed typically by a factor of 2 in the slave-boson approach. Repeating further the

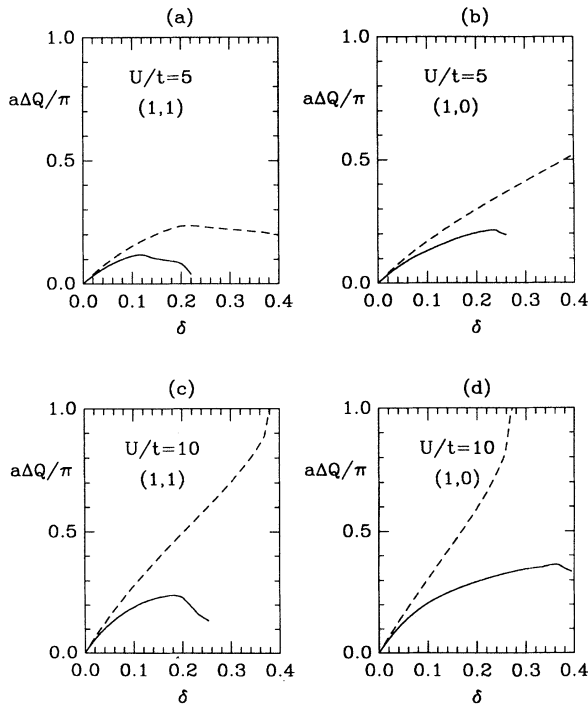


FIG. 5. Spiral pitch parameter $a\Delta Q/\pi$ for the (1,1) and (1,0) spiral phases vs doping δ , for $U/t=5$ and $U/t=10$. Solid line: slave bosons; broken line: Hartree-Fock. Solid lines terminate when the paramagnetic phase sets in.

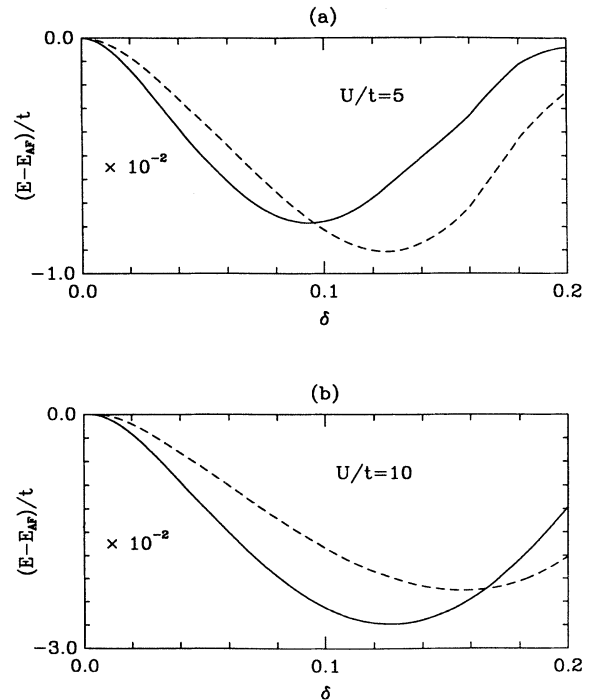


FIG. 6. Energy difference per site (in units of t) between either the (1,1) (solid line) or the (1,0) (broken line) spiral phases and the antiferromagnetic phase vs doping when (a) $U/t=5$ and (b) $U/t=10$.

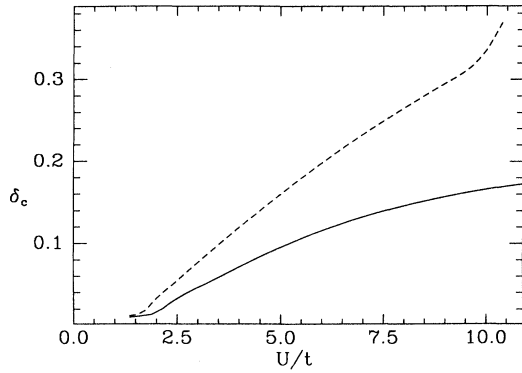


FIG. 7. Critical doping δ_c for the transition from the (1,1) to the (1,0) spiral phase vs U/t . Solid line: slave bosons; broken line: Hartree-Fock (from Fig. 3).

Maxwell construction along the lines discussed in Sec. II and Appendix A to obtain the threshold doping δ^* for the thermodynamic stability of the homogeneous spiral phases, we obtain now $\delta^* \approx 0.14$ when $U/t=5$ and $\delta^* \approx 0.19$ when $U/t=10$. Both values of δ^* correspond now to the (1,0) phase, although the energy difference for this preference is admittedly small. Notice that the calculation of δ^* when $U/t=5$ is now complicated by the occurrence of a secondary minimum of $\mu(\delta)$ for the (1,1) spiral phase.

To analyze the reason why this secondary minimum

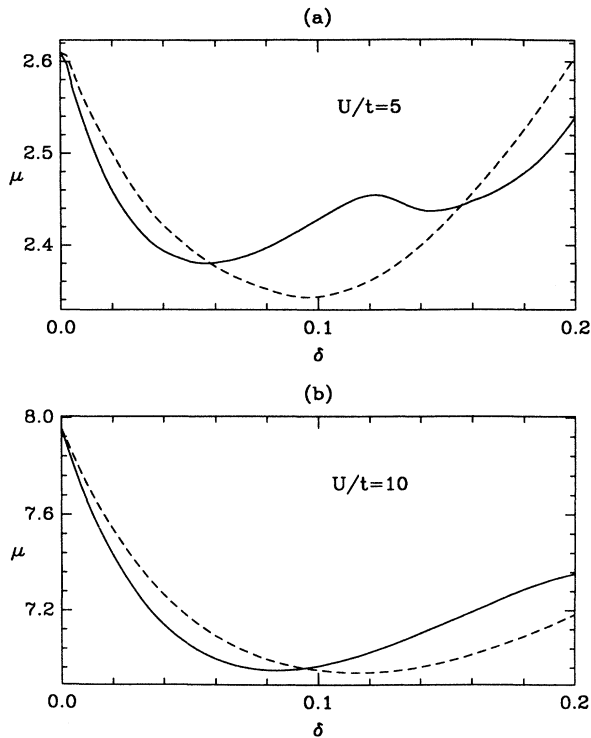


FIG. 8. Chemical potential (in units of t) vs doping when (a) $U/t=5$ and (b) $U/t=10$, for the (1,1) (solid line) and the (1,0) (broken line) spiral phases.

occurs, we have determined numerically the second derivatives of the total energy for each spiral phase in both directions parallel and orthogonal to ΔQ (all other mean-field parameters being determined self-consistently at each Q). Pictorially, these derivatives provide us with a measure of the stiffness of the spiral state against fluctuations of the spiral pitch and of the spiral direction, respectively, in the static and long-wavelength limits. Figure 9 shows these derivatives versus doping when $U/t=5$ for the two spiral phases. Typically, fluctuations in the spiral pitch prove to be “harder” than fluctuations in the spiral direction, thus making it easier for the spiral to tilt than to elongate. In particular, fluctuations in the spiral direction become critical for the (1,1) spiral phase at $\delta \approx 0.12$ (when $U/t=5$), a value that significantly coincides with the onset of the secondary anomalous decrease in the chemical potential of Fig. 8(a). At this doping value, in fact, one eigenvalue of the quadratic fluctuations matrix becomes negative as the second cross derivatives vanish by symmetry. This effect can be interpreted as being a precursor of the biaxial to the uniaxial transition from a helimagnet to a spin nematic recently discussed in Ref. 11. However, a fuller study of the nematic state would require to take into account dynamical fluctuations which are beyond the scope of the present mean-field treatment.

Another piece of information that can be drawn from our approach concerns the distortion upon doping of the characteristic square Fermi surface for a two-dimensional itinerant antiferromagnet at half-filling. The high degeneracy occurring along the magnetic zone boundary at half-filling is, in fact, removed by the spiral distortion of

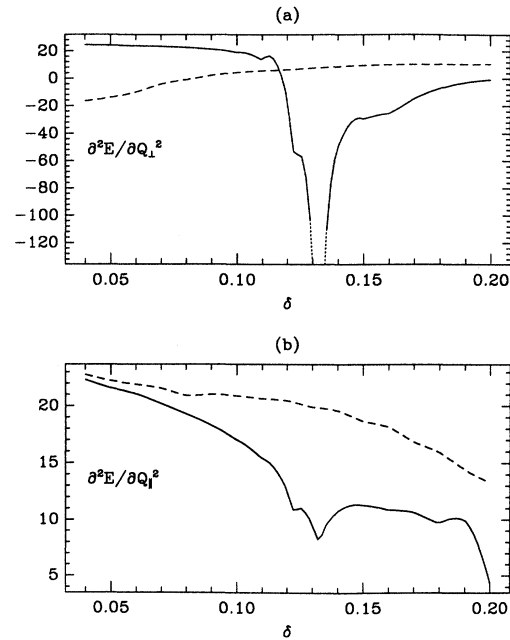


FIG. 9. Second derivatives of the total energy (per site and in units of t) with respect to variations of the total wave vector Q (in units of π/a) (a) transverse to and (b) along the direction of ΔQ vs doping when $U/t=5$. Solid line: (1,1) spiral; broken line: (1,0) spiral.

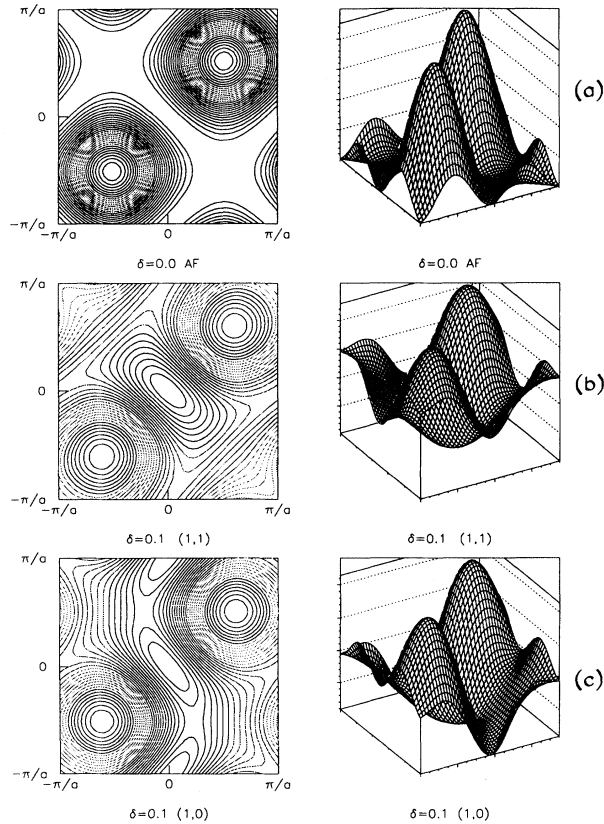


FIG. 10. Constant-energy surfaces and energy dispersion of the upper band when $U/t=5$ for (a) the (undoped) antiferromagnet, (b) the (1,1) spiral phase with $\delta=0.1$, and (c) the (1,0) spiral phase with $\delta=0.1$. Energies are in units of t and wave vectors in units of π/a . The unconventional choice of the Brillouin zone derives from the phase choice of the Bloch operators $d_{k\xi}$ defined by Eq. (2.12) of the text.

the long-range spin order, as shown in Fig. 10 for both spiral phases with $U/t=5$ and $\delta=0.1$. In both cases the minimum of the upper band (namely, the band which is progressively filled by holes upon doping) is seen to occur at the center of the Brillouin zone [corresponding to $\mathbf{k}=(\pi/2a)(\pm 1, \pm 1)$ for the more conventional choice of Brillouin zone], in agreement with perturbative results on spiral states with $\delta=0^+$ and small ΔQ^6 and with RPA self-energy calculations for a single hole in an itinerant antiferromagnet.²⁰ Finally, it can be remarked from the analysis of the band structure that the indirect gap between the two magnetic bands vanishes for doping values close to the minima of Fig. 6. At the same time the chemical potential gets closer to the top of the lower band for increasing doping while remaining attached to the upper band.

IV. CONCLUDING REMARKS

In this paper we have characterized the static properties of the two-dimensional incommensurate spiral spin states by two different mean-field approximations to a single-band Hubbard Hamiltonian. In particular, we

have mostly been concerned with the range of the Hubbard parameter U/t appropriate to weak and intermediate couplings ($U/t \approx 5$) that cannot be covered by calculations based on the t - J model.^{1-2,4,6-8} We have found consistently that the itinerant approach favors the occurrence of the incommensurate phases by enlarging their domain of stability at the expenses of more symmetric phases such as the antiferromagnetic or the ferromagnetic ones. A right variety of phenomena can be run into by our approach. Specifically, we have obtained a competition between alternative spiral phases upon doping and the coexistence in equilibrium over a finite doping range of the antiferromagnetic and the spiral phases, provided obviously that the holes are allowed to phase separate by suitably screening their mutual repulsion. We found it encouraging that the doping values for these phenomena to occur are relevant to the ceramic superconductors when a typical value $U/t \approx 5$ is considered. However, a meaningful comparison with experiments unavoidably requires the inclusion of quantum fluctuations about the mean field we have considered since finite-frequency incommensurate spin correlations have only been detected by neutrons.⁹ The use of a multi-band Hubbard Hamiltonian is further advisable to achieve a more quantitative description of the spiral phases in copper-oxide superconductors, by taking into account the charge-transfer degree of freedom between Cu and O atoms.²¹

We have found, in addition, that the static and long-wavelength fluctuations in the spiral direction lead to an instability of the (1,1) spiral phase beyond a doping threshold (which again is numerically relevant to ceramic superconductors when $U/t \approx 5$). The instability leads to melting of the (1,1) spiral, possibly merging into a moment-free quantum spin nematics.¹¹

Finally, the possible coexistence of the antiferromagnetic and the spiral phases over a finite doping range unavoidably elicits one's speculation about the relevance of the spiral phases for the superconducting mechanism. As the incommensurate phase is allowed to split into randomly distributed disconnected domains which are embedded in the antiferromagnetic phase, interconnection among the domains should only occur when their overall volume exceeds a certain fraction of the total sample volume. In this context, it would be significant to determine whether this condition enables superconductivity to set in the whole sample.

An attempt to relate the presence of spiral phases with superconductivity has recently been presented within a spin model.²² In this model, spin-fluctuation-induced pairing results from the tendency of the off-spiral-plane fluctuations to reduce the frustration energy. It remains to be verified, however, whether this magnetic pairing and the hole pairing needed for superconductivity can be identified within a localized spin model. This remark points out the importance of including fluctuations in the present itinerant approach.

ACKNOWLEDGMENTS

We are indebted to M. Geddo for computational support during the initial stage of this work and to G. Jug

for discussions. One of us (E.A.) gratefully acknowledges research support from Europa Metall-LMI s.p.a.

APPENDIX A: MAXWELL CONSTRUCTION FOR THE ANOMALOUS DECREASE OF THE CHEMICAL POTENTIAL WITH DOPING

The anomalous decrease of the chemical potential with doping shown in Figs. 4 and 8 of the text is a signal that the system finds it thermodynamically more convenient to phase separate into two subsystems with different den-

$$F(T, V, N; V_1, N_1) = V_1 f \left[T, N_1/V_1 \right] + (V - V_1) f(T, (N - N_1)/(V - V_1)) \quad (\text{A1})$$

can then be minimized with respect to N_1 and V_1 to yield

$$\mu(T, \delta_1) = \mu(T, \delta_2), \quad (\text{A2})$$

$$f(T, \delta_2) - f(T, \delta_1) = (\delta_2 - \delta_1) \mu(T, \delta_1),$$

where $\delta_1 = N_1/V_1$ and $\delta_2 = N_2/V_2$. Let

$$x = (\delta - \delta_2)/(\delta_2 - \delta_1) \quad (\text{A3})$$

with $0 \leq x \leq 1$ for $\delta_1 \leq \delta \leq \delta_2$. The free energy (A1) can thus be cast in the form

$$F(T, V; x) = V[(1-x)f(T, \delta_1) + xf(T, \delta_2)] \\ = V[f(T, \delta_1) + (\delta - \delta_1)\mu(T, \delta_1)]. \quad (\text{A4})$$

A graphical construction (known as a Maxwell construc-

tion) suffices to determine the two densities δ_1 and δ_2 from Eqs. (A2), and to show that the free energy (A4) for two phases coexisting in equilibrium is lower than the free energy $Vf(T, \delta)$ for a single phase of density $\delta = N/V$ whenever $\delta_1 < \delta < \delta_2$ (cf. Fig. 11).

Quite generally, we assume that $\mu(\delta)$ behaves schematically as shown in Fig. 11. At given temperature T , we then suppose that the system breaks up into two subsystems with volumes V_1 and V_2 and number of particles N_1 and N_2 , respectively, such that $V_1 + V_2 = V$ and $N_1 + N_2 = N$ are kept constant. The corresponding free energy

tion) suffices to determine the two densities δ_1 and δ_2 from Eqs. (A2), and to show that the free energy (A4) for two phases coexisting in equilibrium is lower than the free energy $Vf(T, \delta)$ for a single phase of density $\delta = N/V$ whenever $\delta_1 < \delta < \delta_2$ (cf. Fig. 11).

The actual behavior of $\mu(\delta)$ shown in Figs. 4 and 8 of the text for the two spiral phases (1,1) and (1,0) is slightly more complicated than the prototype behavior considered in Fig. 11. In particular: (i) the chemical potential is discontinuous at $\delta=0$ as it jumps across the antiferromagnetic gap; (ii) a secondary minimum can occur for the (1,1) phase; (iii) the chemical potential drops discontinuously from the (1,1) to the (1,0) phase at δ_c . The Maxwell construction of Fig. 11 can nonetheless be generalized to include these novel features. In all cases one obtains $\delta_1=0$ while $\delta_2=\delta^*$ is given in the text for two representative values of U/t . Notice that the Maxwell construction pins now the chemical potential within the energy gap of the antiferromagnetic phase.

APPENDIX B: ROTATIONALLY INVARIANT SLAVE-BOSON APPROACH

Spin-rotational invariance is a fundamental property of the interaction term of the Hubbard Hamiltonian, and any functional integral formulation of the partition function based on the Hubbard Hamiltonian would preserve the invariance if no approximations were performed. Approximations may introduce, however, spurious results which violate spin-rotational invariance; a correct functional integral formulation should then preserve the invariance at any level of approximations. This problem has been debated for the functional integral formulations of the Hubbard Hamiltonian that rely on the Hubbard-Stratonovitch transformation²⁴ and, more recently, also for the Kotliar-Ruckenstein slave-boson formulation.²⁵ The latter has been generalized by considering four (instead of two) s -like slave bosons which transform as a spin matrix under spin rotations and by introducing two additional constraints,²⁵ thereby effectively averaging over all possible basis sets for spin $\frac{1}{2}$ with different orientations of the quantization axis.

The formulation of Ref. 25 for slave bosons, and more explicitly the one of Ref. 7 based on the Hubbard-Stratonovitch transformation, introduces the averaging over the different orientations of the quantization axis at each point in space *and* imaginary time. The slave-boson

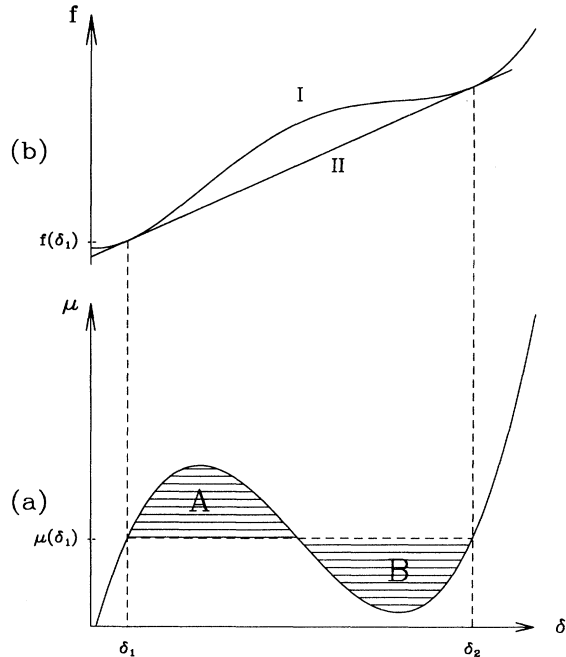


FIG. 11. (a) Schematic plot of the chemical potential vs doping showing an anomalous decrease between a local maximum and a local minimum. Maxwell construction equates the areas of the two shaded regions marked A and B. (b) Corresponding free energy density vs doping for (I) a single homogeneous phase with density δ and (II) two phases with densities δ_1 and δ_2 coexisting in equilibrium.

approach with variable quantization axes that we have discussed in Sec. III, on the other hand, is compatible with the functional integral formulation provided the quantization axes do not fluctuate in time (spatial fluctuations are instead readily introduced by averaging the functional integral over all possible sets $\{\Omega_i\}$, independently at each site i). Nonetheless, we shall show that the introduction of quantization axes which can only fluctuate in space is sufficient to render the Kotliar-Ruckenstein slave-boson approach manifestly spin-rotationally invariant.

To show this we consider the calculation of the longitudinal and transverse parts of the (equal time) spin correlation function $\langle \mathbf{S}_i \cdot \mathbf{S}_j \rangle$ at different sites. Although in the paramagnetic phase these two parts must coincide, the Kotliar-Ruckenstein formulation violates this property at the lowest order for the vertices associated with the mapping (3.2) (and for fixed quantization axes). In the slave-boson representation of Ref. 12, we can in fact map the product $\mathbf{S}_i \cdot \mathbf{S}_j$ into the following operator:

$$\begin{aligned} \mathbf{S}_i \cdot \mathbf{S}_j \rightarrow & \frac{1}{2} \sum_{\sigma} z_{i\sigma}^\dagger z_{i\bar{\sigma}} c_{i\sigma}^\dagger c_{i\bar{\sigma}} z_{j\bar{\sigma}}^\dagger z_{j\sigma} c_{j\bar{\sigma}}^\dagger c_{j\sigma} \\ & + \frac{1}{2} \sum_{\sigma} \sigma z_{i\sigma}^\dagger z_{i\sigma} c_{i\sigma}^\dagger c_{i\sigma} \frac{1}{2} \sum_{\sigma'} \sigma' z_{j\sigma'}^\dagger z_{j\sigma'} c_{j\sigma'}^\dagger c_{j\sigma'} . \end{aligned} \quad (\text{B1})$$

Upon exploiting the constraints, each pair of bosonic z operators at the same site with *equal* spin projections in the last term of Eq. (B1) can be replaced by unity [in agreement to what was done in the first term on the right-hand side of Eq. (3.3) of the text]. In the first term of Eq. (B1), on the other hand, where the pairs of z operators at the same site occur with *opposite* spin projections, this replacement cannot be done. When the average of $\mathbf{S}_i \cdot \mathbf{S}_j$ is evaluated at the lowest order by replacing the z factors with their mean-field value, a difference between the longitudinal and transverse parts of the spin correlation function unavoidably results even in the paramagnetic phase.

This shortcoming of the Kotliar-Ruckenstein method can be overcome upon averaging over all possible realizations of the spin quantization axis at each lattice site. To this end we write the spin operators in the form $(\alpha, \beta = x, y, z)$:

$$\begin{aligned} S_i^{(\alpha)} \rightarrow & (1-z^2)^{\frac{1}{2}} \sum_{\sigma, \sigma'} c_{i\sigma}^\dagger T_{\alpha z}(\Omega_i) \sum_{\xi, \xi'} [\mathcal{R}(\Omega_i)]_{\sigma\xi} \sigma_{\xi\xi}^{(z)} [\mathcal{R}^\dagger(\Omega_i)]_{\xi'\sigma'} c_{i\sigma'} \\ & + z^2 \frac{1}{2} \sum_{\sigma, \sigma'} c_{i\sigma}^\dagger \sum_{\beta} T_{\alpha\beta}(\Omega_i) \sum_{\xi, \xi'} [\mathcal{R}(\Omega_i)]_{\sigma\xi} \sigma_{\xi\xi}^{(\beta)} [\mathcal{R}^\dagger(\Omega_i)]_{\xi'\sigma'} c_{i\sigma'} \\ = & (1-z^2)^{\frac{1}{2}} \sum_{\sigma, \sigma'} c_{i\sigma}^\dagger T_{\alpha z}(\Omega_i) \sum_{\beta} \sigma_{\sigma\sigma'}^{(\beta)} T_{\beta z}(\Omega_i) c_{i\sigma'} + z^2 \frac{1}{2} \sum_{\sigma, \sigma'} c_{i\sigma}^\dagger \sigma_{\sigma\sigma'}^{(\alpha)} c_{i\sigma'} , \end{aligned} \quad (\text{B7})$$

where use has been made of the inverse of transformation (B3). Performing finally the spherical average separately at each site, Eq. (B7) is replaced for *any* α by

$$\int \frac{d\Omega_i}{4\pi} S_i^{(\alpha)} \rightarrow \left[\frac{1+2z^2}{3} \right] \frac{1}{2} \sum_{\sigma, \sigma'} c_{i\sigma}^\dagger \sigma_{\sigma\sigma'}^{(\alpha)} c_{i\sigma'} \quad (\text{B8})$$

since [cf. Eq. (B4)]

$$\begin{aligned} S_i^{(\alpha)} &= \frac{1}{2} \sum_{\sigma, \sigma'} c_{i\sigma}^\dagger \sigma_{\sigma\sigma'}^{(\alpha)} c_{i\sigma'} \\ &= \frac{1}{2} \sum_{\xi, \xi'} d_{i\xi}^\dagger \left[\sum_{\xi, \xi'} [\mathcal{R}^\dagger(\Omega_i)]_{\xi\sigma} \sigma_{\sigma\sigma'}^{(\alpha)} [\mathcal{R}(\Omega_i)]_{\sigma'\xi'} \right] d_{i\xi'} \\ &= \frac{1}{2} \sum_{\xi, \xi'} d_{i\xi}^\dagger \sum_{\beta} T_{\alpha\beta}(\Omega_i) \sigma_{\xi\xi'}^{(\beta)} d_{i\xi'} , \end{aligned} \quad (\text{B2})$$

where use has been made of the transformation (2.2) and of the associated transformation property of the Pauli matrices

$$\mathcal{R}^\dagger(\Omega_i) \sigma^{(\alpha)} \mathcal{R}(\Omega_i) = \sum_{\beta} T_{\alpha\beta}(\Omega_i) \sigma^{(\beta)} . \quad (\text{B3})$$

Here

$$T(\Omega) = \begin{bmatrix} \cos\theta \cos\varphi & -\sin\varphi & \sin\theta \cos\varphi \\ \cos\theta \sin\varphi & \cos\varphi & \sin\theta \sin\varphi \\ -\sin\theta & 0 & \cos\theta \end{bmatrix} \quad (\text{B4})$$

rotates the \hat{z} axis into the local quantization axis specified by the spherical angles Ω . Performing at this point the mapping (3.2) via the slave-boson representation, Eq. (B2) becomes then

$$\begin{aligned} S_i^{(\alpha)} \rightarrow & \frac{1}{2} \sum_{\xi, \xi'} d_{i\xi}^\dagger T_{\alpha z}(\Omega_i) \sigma_{\xi\xi'}^{(z)} d_{i\xi'} \\ & + \frac{1}{2} \sum_{\xi, \xi'} d_{i\xi}^\dagger z_{i\xi}^\dagger \sum_{\beta=x,y} T_{\alpha\beta}(\Omega_i) \sigma_{\xi\xi'}^{(\beta)} z_{i\xi'} d_{i\xi'} , \end{aligned} \quad (\text{B5})$$

where again the pair of bosonic z operators with equal spin projection have been replaced by unity. Within the saddle-point approximation for the z operators in the paramagnetic phase, Eq. (B5) further reduces to

$$\begin{aligned} S_i^{(\alpha)} \rightarrow & (1-z^2)^{\frac{1}{2}} \sum_{\xi, \xi'} d_{i\xi}^\dagger T_{\alpha z}(\Omega_i) \sigma_{\xi\xi'}^{(z)} d_{i\xi'} \\ & + z^2 \frac{1}{2} \sum_{\xi, \xi'} d_{i\xi}^\dagger \sum_{\beta} T_{\alpha\beta}(\Omega_i) \sigma_{\xi\xi'}^{(\beta)} d_{i\xi'} . \end{aligned} \quad (\text{B6})$$

To evaluate the average over Ω_i , it is convenient to transform back to the \hat{z} quantization axis by exploiting the independence of the action in the functional integral on the particular quantization axis for the paramagnetic phase. One obtains²⁶

$$\int \frac{d\Omega_i}{4\pi} T_{\alpha z}(\Omega_i) T_{\beta z}(\Omega_i) = \frac{1}{3} \delta_{\alpha\beta} . \quad (\text{B9})$$

In this way the correct isotropy of the spin correlation function $\langle \mathbf{S}_i \cdot \mathbf{S}_j \rangle$ has been restored. A similar result follows from the spin-rotation-invariant approach of Ref. 25.

- ¹B. L. Shraiman and E. D. Siggia, *Phys. Rev. Lett.* **62**, 1564 (1989).
- ²C. Jayaprakash, H. R. Krishnamurthy, and S. Sarker, *Phys. Rev. B* **40**, 2610 (1989).
- ³J. Zaanen and O. Gunnarsson, *Phys. Rev. B* **40**, 7391 (1989).
- ⁴C. L. Kane, P. A. Lee, T. K. Ng, B. Chakraborty, and N. Read, *Phys. Rev. B* **41**, 2653 (1990).
- ⁵H. J. Schulz, *Phys. Rev. Lett.* **64**, 1445 (1990).
- ⁶Z. Y. Weng and C. S. Ting, *Phys. Rev. B* **42**, 803 (1990).
- ⁷H. J. Schulz, *Phys. Rev. Lett.* **65**, 2462 (1990).
- ⁸P. Hedegård and M. B. Pedersen, *Phys. Rev. B* **42**, 10035 (1990).
- ⁹T. R. Thurston *et al.*, *Phys. Rev. B* **40**, 4585 (1989), and references cited therein.
- ¹⁰Phase separation of holes in an antiferromagnet has been already considered within the t - J model by V. J. Emery, S. A. Kivelson, and H. Q. Lin [*Phys. Rev. Lett.* **64**, 475 (1990)], who have also suggested that phase separation can become possible despite the Coulomb repulsion among the holes because of the screening provided by the quite mobile negatively charged oxygen ions.
- ¹¹P. Chandra and P. Coleman, *Phys. Rev. Lett.* **66**, 100 (1991); see also L. P. Gor'kov and A. V. Sokol, *Pis'ma Zh. Eksp. Teor. Fiz.* **52**, 1103 (1990) [*JETP Lett.* **52**, 394 (1990)].
- ¹²G. Kotliar and A. E. Ruckenstein, *Phys. Rev. Lett.* **57**, 1362 (1986).
- ¹³More complex spin arrangements such as the double-spiral state proposed in Ref. 4 are outside the scope of the present treatment since they do not maintain long-range order.
- ¹⁴For the general spiral states which result from these two conditions the local number density is site independent. Linearly polarized incommensurate spin-density waves where the spins do not cant, on the other hand, are accompanied by a charge-density wave representing the local density of excess holes (cf. Refs. 3 and 5).
- ¹⁵B. R. Cooper, R. J. Elliott, S. J. Nettel, and H. Suhl, *Phys. Rev.* **127**, 57 (1962).
- ¹⁶The connection between incommensurate antiferromagnetism and hole mobility, which has been noticed experimentally (Ref. 9), has been interpreted as a clue in favor of the occurrence of *spiral* phases.
- ¹⁷It has recently been shown with a renormalized random-phase-approximation calculation [L. Chen, C. Bourbonnais, T. Li, and A.M.S. Tremblay, *Phys. Rev. Lett.* **66**, 369 (1991)] that the Stoner ferromagnetic phase can completely disappear when the effective hard-core repulsion introduced by electron correlation for large U is taken into account.
- ¹⁸L. Lilly, A. Muramatsu, and W. Hanke, *Phys. Rev. Lett.* **65**, 1379 (1990).
- ¹⁹E. Arrigoni, G. Strinati, and C. Castellani, *Phys. Rev. B* **41**, 4838 (1990).
- ²⁰G. Vignale and M. R. Hedayati, *Phys. Rev. B* **42**, 786 (1990). It has been shown, however, by exact diagonalization of small clusters [D. Poilblanc and E. Dagotto, *Phys. Rev. B* **42**, 4861 (1990)] that two-hole correlations act to redistribute the holes on the Fermi surface, favoring the existence of hole pockets near the corners at $(\pi/a)(1,0)$ and $(\pi/a)(0,1)$.
- ²¹V. J. Emery, *Phys. Rev. Lett.* **58**, 2794 (1987).
- ²²G. Jug, *J. Phys. Condens. Matter* **3**, 1211 (1991).
- ²³See, e.g., K. Huang, *Statistical Mechanics* (Wiley, New York, 1963).
- ²⁴A. A. Gomes and P. Lederer, *J. Phys. (Paris)* **38**, 231 (1977), and references cited therein; see also Ref. 7.
- ²⁵T. Li, P. Wölfle, and P. J. Hirschfeld, *Phys. Rev. B* **40**, 6817 (1989).
- ²⁶Although we use in the following the same notation $c_{i\sigma}$ as in Eq. (2.2) for the back-transformed operators, the operators $c_{i\sigma}$ in Eqs. (B7) and (B8) do not coincide with the original fermion operators of the Hubbard Hamiltonian (2.1).